





Novel Methodology for Integrated Actuator and Sensors Fault Detection and Estimation in an Active Suspension System

Miguel Meléndez-Useros , *Student Member, IEEE*, Manuel Jiménez-Salas , *Student Member, IEEE*,
Fernando Viadero-Monasterio , *Member, IEEE*, and María Jesús López-Boada 

Abstract—In recent years, there has been a great deal of interest in the development of fault detection and isolation (FDI) techniques because they have been found to be important in road transport systems to ensure safe operation, reliability, and maintainability. Active suspension systems (ASSs) play an important role in passengers vehicles, especially in autonomous vehicles, because they can adapt based on the information provided by on-board sensors, thereby improving passengers' comfort and safety. However, the possible occurrence of faults in critical components, such as actuators and sensors requires robust fault diagnosis schemes to ensure good system performance and reliability. Numerous investigations exist on identification and estimation of sensor and actuator faults in ASSs, but faults in both types of components are never considered. This article proposes a new fault diagnosis scheme that allows integrated detection and estimation of actuator and sensors faults in ASSs. The proposed methodology uses two unknown input observers (UIOs) to estimate actuator faults and sensor faults separately. To avoid coupling between the estimations, it is also proposed a switch OFF mechanism for the actuator so that the coupled deflection sensor and actuator faults can be distinguished and isolated. Finally, signal flags are generated to distinguish the faulty suspension component and refine the UIO estimations.

Index Terms—Active suspension, actuator fault estimation, fault diagnosis, sensors faults estimation, unknown input observer (UIO), vehicle safety.

I. INTRODUCTION

FAULT detection and isolation (FDI) techniques have gained considerable attention in recent years as they have been shown to play a vital role in many real-world systems and industries, improving safety and extending equipment lifetime. The main purpose of the FDI techniques is to detect when there exists some fault [fault detection (FD)], and then to determine the location of the fault [fault isolation (FI)], so that some action can be taken to eliminate or minimize its effect [fault tolerant control (FTC)] [1].

Manuscript received 27 November 2023; revised 8 February 2024 and 14 March 2024; accepted 11 April 2024. This work was supported in part by MCIN/AEI/ 10.13039/501100011033 under Grant [PID2022-136468OB-I00] and in part by the “ERDF A way of making Europe.” Associate Editor: Qiang Miao. (*Corresponding author: Miguel Meléndez-Useros.*)

The authors are with the Department of Mechanical Engineering, University Carlos III de Madrid, 28911 Madrid, Spain (e-mail: mmelende@ing.uc3m.es; manuejim@ing.uc3m.es; fviadero@ing.uc3m.es; mjboada@ing.uc3m.es).

Digital Object Identifier 10.1109/TR.2024.3389290

The suspension system plays an important role in a vehicle because it influences both the comfort and safety of passengers [2]. To overcome the limits of traditional passive suspensions, more advanced technologies consisting of controlled suspensions, such as active and semi-active ones, have been researched for decades. These suspension systems offer better performance regarding ride comfort and road holding [3], [4], [5], [6], [7], [8] as they can adapt to the situation using the information provided by on-board sensors and perform vibration suppression. Jurisch [9] lists the potential of active suspension for autonomous vehicles (AVs), which are becoming increasingly prominent in our society. Many control approaches have been used to design controllers for both active and semi-active systems, such as \mathcal{H}_∞ control or linear quadratic regulator control [10], [11], [12], [13], [14], [15]. Nowadays, the use of model predictive control (MPC) is experiencing a significant increment due to its ability to predict the future behavior of the controlled system and to handle constraints on inputs, states, and outputs [16], [17].

The effectiveness of control over the suspension system relies on the performance of the sensors and actuators. However, when working with real systems, it is unavoidable that faults occur on these components [18], affecting the operation of the controllers and the performance of the suspension system [19]. For that reason, extensive research works focus on FTC methodologies to design controllers for suspension systems that ensure the stability and safety of the vehicle. Some FTC designs are robust to faults but do not have any information about the fault [20], [21], [22], resulting in limitations in their performance. A more active perspective consists of designing controllers that use the estimation of the faults, [fault estimation (FE)] to carry out their control task [23], [24]. Using FDI and FE techniques, faults can be detected and estimated. Hardware redundancy approaches use duplicated sensors to detect faults with a high level of accuracy and stability but the need for more components increases the space required and the cost. Analytic redundancy methods [25], [26], [27] use information about the inputs and outputs of the system by knowing the relationship between them from the dynamics of the system when it is operating without any fault. Residual techniques use this relationship to detect faults when the value of the defined residuals exceeds the value of a predefined threshold [28], [29], [30], [31]. Other studies use model-based observers to estimate the value of the

fault [32], [33], [34]. In [35] and [36], a robust unknown input observer (UIO) is used to estimate faults in the actuators of a semi-active suspension. The use of a bank of observers is a common approach to detect faults as it can be seen in [37], where a bank of sliding mode observers is used to detect faults in sensors of a full suspension system while in [38] and [39] bank of extended and unscented Kalman filters is used for the same purpose. The \mathcal{H}_∞ approach is also used to design robust observers for FD in suspension systems in [40] and [41] so that the close-loop effect of the disturbances over the estimations are minimized following the \mathcal{H}_∞ criteria. In [42], observers based on genetic algorithms (GAs) have been also used to detect faults in suspensions.

However, all the mentioned works can only detect and/or estimate either sensor faults or actuator faults, but never in both. In addition, the effects of sensor and actuator faults are coupled in an active suspension system (ASS) because a fault in the actuator will affect the sensor signal and thus the strong detectability condition is not satisfied [43], [44], leading to situations in which the origin of the fault cannot be identified. This implies that a component can be identified as faulty when the actual fault comes from a different component, resulting in poor system performance or even causing system instability. This highlights the need to design a methodology to detect or estimate faults in any of the sensors and actuators of the ASS.

Motivated for the aforementioned reasons, in this article, a novel methodology based on UIO is proposed to detect and estimate faults in both sensors and actuator found in series-production vehicles. Since deflection sensor faults and actuator faults have similar effects on the UIOs estimations, they cannot be distinguished by means of them. To handle the coupling issue, it is proposed to perform a momentary shutdown of the actuator to check if the fault persists and to distinguish the origin of the fault. Once the fault is isolated, a detection flag is generated so that the faulty component can be identified, always under the assumption that no more of one fault can occur at the same time. Finally, the detection flag is used to correct the values of the estimations performed by the UIOs.

Specifically, the main contributions of this work are as follows.

- 1) A new methodology is proposed for the estimation of both actuator and sensor faults for an ASS by using two robust UIOs based on the \mathcal{H}_∞ criteria in order to present robustness against road disturbances.
- 2) Using the estimation of the UIOs, FD flags are generated using a new proposed switch off mechanism of the actuator. In this way, coupled faults can be distinguished.
- 3) The generated detections flags are used to refine the estimations of the UIOs in order to avoid false estimations due to coupling between actuator and sensor faults using a new proposed estimation logic masking system.

Finally, the proposed methodology is validated in both a quarter suspension vehicle model and a complex vehicle model in *CarSim*.

The rest of the article is organized as follows: in Section II, the formulation of the problem is presented as well as the quarter vehicle model used for the design of the observers. In addition,

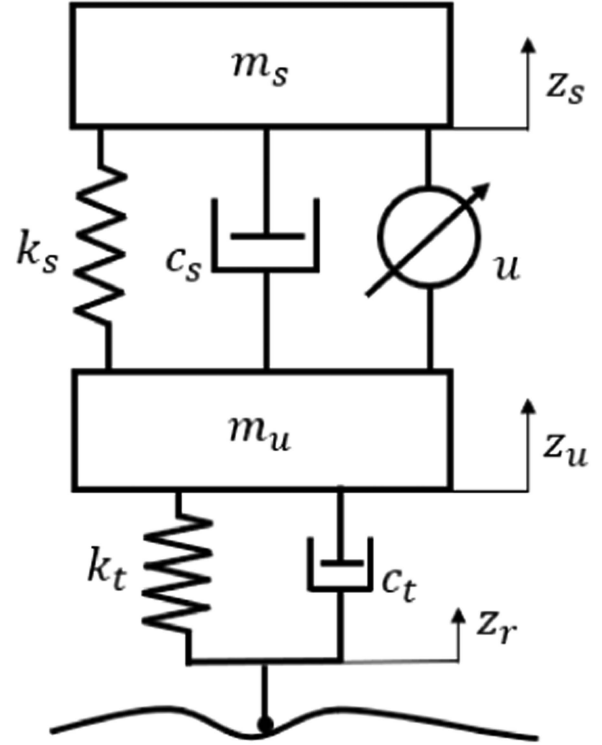


Fig. 1. Quarter vehicle model representation.

the detectability conditions for the ASS faults are described in this section. The novel fault diagnosis scheme, the derivation of the robust UIOs and the flag generation for the FD are presented in Section III. To prove the operation of the designed fault diagnosis scheme, simulations are carried out considering two system plants: 1) a quarter suspension vehicle model in *Matlab* and 2) a 27-DoF vehicle model from *CarSim*, Section IV. Finally, Section V concludes this article.

Notation: In this article, “ \top ” represents the transpose operator and “ \star ” stands for a symmetric term in a matrix, $X \succ 0$ states that matrix X is positive definite. If the dimensions of matrices are not indicated, they are supposed to have compatible dimensions.

II. SYSTEM MODEL AND PROBLEM FORMULATION

A. ASS Model

In this article, a linear quarter-vehicle suspension model [45] is used for the design of the controller and the FDI problem as depicted in Fig. 1.

The equations that determine the dynamics of the model shown in Fig. 1 are as follows:

$$\begin{aligned}
 m_s \ddot{z}_s(t) &= -k_s(z_s(t) - z_u(t)) \\
 &\quad - c_s(\dot{z}_s(t) - \dot{z}_u(t)) + u(t) \\
 m_u \ddot{z}_u(t) &= k_u(z_u(t) - z_r(t)) + c_s(\dot{z}_s(t) - \dot{z}_u(t)) \\
 &\quad - u(t) - k_u(z_u(t) - z_r(t)) \\
 &\quad - c_u(\dot{z}_u(t) - \dot{z}_r(t))
 \end{aligned} \tag{1}$$

where $z_s(t)$ and $z_u(t)$ are the displacement of the sprung mass and unsprung mass, respectively; $z_r(t)$ is the road profile over time; $u(t)$ is the control force input of the actuator; k_s and k_u are the stiffness of the suspension spring and tire, respectively; c_s and c_u are the damping coefficient of the suspension and tire, respectively; and m_s and m_u are the sprung and unsprung mass, respectively. Equation (1) is expressed in state-space form as

$$\begin{aligned}\dot{x}(t) &= Ax(t) + Bu(t) + B_\omega\omega(t) \\ y(t) &= Cx(t) + Du(t) + D_\omega\omega(t)\end{aligned}\quad (2)$$

where

$$\begin{aligned}A &= \begin{bmatrix} 0 & 0 & 1 & -1 \\ 0 & 0 & 0 & 1 \\ -\frac{k_s}{m_s} & 0 & -\frac{c_s}{m_s} & \frac{k_s}{m_s} \\ \frac{k_s}{m_u} & -\frac{k_u}{m_u} & \frac{c_s}{m_u} & -\frac{(c_s+c_u)}{m_u} \end{bmatrix}, \quad B_u = \begin{bmatrix} 0 \\ 0 \\ \frac{1}{m_s} \\ -\frac{1}{m_u} \end{bmatrix} \\ B_\omega &= \begin{bmatrix} 0 \\ -1 \\ 0 \\ -\frac{c_u}{m_u} \end{bmatrix}, \quad C = \begin{bmatrix} 1 & 0 & 0 & 0 \\ -\frac{k_s}{m_s} & 0 & -\frac{c_s}{m_s} & \frac{k_s}{m_s} \\ \frac{k_s}{m_u} & -\frac{k_u}{m_u} & \frac{c_s}{m_u} & -\frac{(c_s+c_u)}{m_u} \end{bmatrix} \\ D &= \begin{bmatrix} 0 \\ \frac{1}{m_s} \\ \frac{1}{m_u} \end{bmatrix}, \quad D_\omega = \begin{bmatrix} 0 \\ 0 \\ -\frac{c_u}{m_u} \end{bmatrix}\end{aligned}\quad (3)$$

and $x(t) = [\Delta_z(t) \ \Delta_{zt}(t) \ \dot{z}_s(t) \ \dot{z}_u(t)]^\top$ is the state vector of the system consisting of suspension deflection ($\Delta_z(t) = z_s(t) - z_u(t)$), tire deflection ($\Delta_{zt}(t) = z_u(t) - z_r(t)$), sprung mass velocity, and unsprung mass velocity, respectively. The disturbance input caused by road irregularities is denoted as $\omega(t) = \dot{z}_r(t)$. The measurements given by the sensors are $y(t) = [\Delta_z(t) \ \dot{z}_s(t) \ \dot{z}_u(t)]^\top$, where the suspension deflection can be measured using a linear variable differential transformer and the vertical acceleration of sprung and unsprung mass can be measured using accelerometers [46]. System in (2) is discretized as follows:

$$\begin{aligned}x(k+1) &= A_d x(k) + B_d u(k) + B_{d,\omega} \omega(k) \\ y(k) &= Cx(k) + Du(k) + D_\omega \omega(k)\end{aligned}\quad (4)$$

where

$$A_d = I + T_s A, \quad B_d = T_s B, \quad B_{d,\omega} = T_s B_\omega$$

and T_s is the sample time.

B. Active Suspension Model With Sensor and Actuator Faults

In this study, the faults considered in both sensors and actuators are additive [31]. The state-space model described in (2) is rewritten including the faults in sensors and actuators as

$$\begin{aligned}\dot{x}(t) &= Ax(t) + Bu(t) \\ &\quad + B_\omega\omega(t) + Bf_a(t) \\ y(t) &= Cx(t) + Du(t) \\ &\quad + D_\omega\omega(t) + Df_a(t) + f_s(t)\end{aligned}\quad (5)$$

where $f_s = [f_{\Delta_z} \ f_{\dot{z}_s} \ f_{\dot{z}_u}]^\top$ represents the sensors faults and f_a represents the actuator fault.

C. Detectability Analysis of Simultaneous Actuators and Sensor Faults in ASS

In order to know whether it is possible to detect all potential faults in the system, which are unknown system entries, it is necessary to check the conditions of strong and strong^(*) detectability [47], [48]. These conditions establish the necessary requirements for estimating the states and the unknown inputs of the dynamic system. Redefining the system in (5) using $f(t) = [f_a(t) \ f_s^\top(t)]^\top$ leads to

$$\begin{aligned}\dot{x}(t) &= Ax(t) + Bu(t) + B_\omega\omega(t) + \bar{B}f(t) \\ y(t) &= Cx(t) + Du(t) + D_\omega\omega(t) + \bar{D}f(t)\end{aligned}\quad (6)$$

where

$$\bar{B} = [B \ 0], \quad \bar{D} = [D \ I].\quad (7)$$

Definition 1 (see[47]): The system (6) is strong detectable if $y(t) = 0$ for $t \geq 0$ implies $\lim_{t \rightarrow +\infty} x(t) = 0$ for any given initial state $x(0)$ and fault $f(t) = [f_a(t) \ f_s^\top(t)]^\top$. Strong detectability conditions correspond to the minimal-phase condition.

Definition 2 (see[47]): The system (6) is strong^(*) detectable if $\lim_{t \rightarrow +\infty} y(t) = 0$ implies $\lim_{t \rightarrow +\infty} x(t) = 0$ for any given initial state $x(0)$ and fault $f(t) = [f_a(t) \ f_s^\top(t)]^\top$.

Theorem 1 (see[47]): The quadruple (A, \bar{B}, C, \bar{D}) of the system (6) is strong and strong^(*) detectable if and only if:

- 1) The following rank match condition is satisfied for (A, \bar{B}, C, \bar{D}) :

$$\begin{aligned}\text{rank} \left(\begin{bmatrix} C\bar{B} & 0 & \bar{D} & I \\ \bar{D} & I & 0 & 0 \end{bmatrix} \right) &= \text{rank} \left(\begin{bmatrix} \bar{D} & E \end{bmatrix} \right) \\ &\quad + \text{rank} \left(\begin{bmatrix} \bar{B} & 0 \\ \bar{D} & I \end{bmatrix} \right).\end{aligned}\quad (8)$$

- 2) Minimum-phase condition is satisfied for (A, \bar{B}, C, \bar{D})

$$\begin{aligned}\text{rank} \left(\begin{bmatrix} sI - A & -\bar{B} & 0 \\ C & \bar{D} & I \end{bmatrix} \right) \\ = n + \text{rank} \left(\begin{bmatrix} \bar{B} & 0 \\ \bar{D} & I \end{bmatrix} \right)\end{aligned}\quad (9)$$

where n is the number of states of the system, $s \in \mathbb{C}$ and $\text{Re}(s) \geq 0$.

Both conditions of Theorem 1 are satisfied if and only if [43]

$$n_{f_a} + n_{f_s} \leq m\quad (10)$$

where m is the number of measurements, n_{f_a} is the number of actuator faults, and n_{f_s} is the number of sensor faults. As in the considered case, all sensors are susceptible to being faulty, condition (10) cannot be satisfied, and thus the system (6) does not satisfy the requirement of strong and strong^(*) detectability and there exists a coupling between faults. Therefore, no observer or residual generator allows the detection or estimation of all the system faults. For this reason, in this work, a new methodology

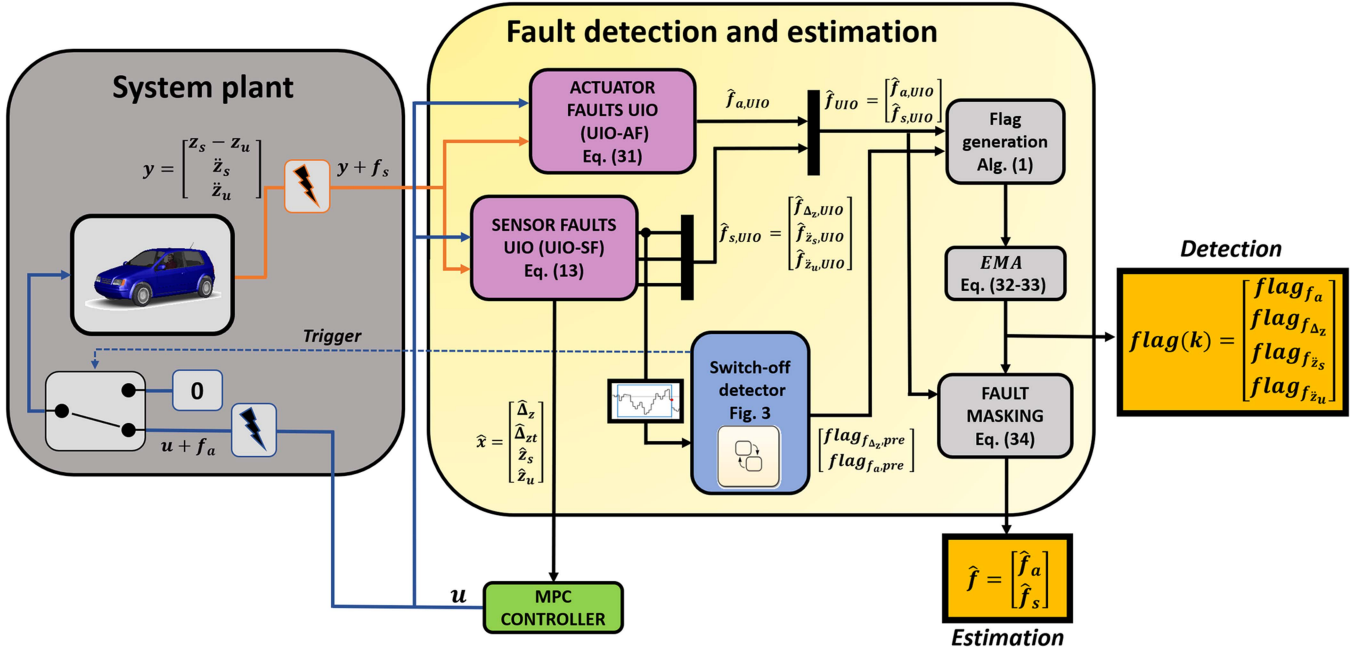


Fig. 2. Proposed fault diagnosis methodology for an ASS.

based on two separate UIOs is proposed to address the issue of detecting and estimating faults in both the actuator and the sensors of an ASS.

III. NOVEL FAULT DIAGNOSIS METHODOLOGY

This section describes the proposed fault diagnosis methodology for simultaneous actuator and sensor faults detection and estimation for an ASS. First, two separate observers for the estimation of the actuator and sensor faults are designed. Then, the coupling between faults estimation problem is described and the switch OFF mechanism is presented. Finally, the FD flags are generated and the detection logic masking system decides whether the estimation given by the UIO is valid, thus avoiding possible false negatives due to coupling between faults. The fault diagnosis methodology for the ASS is depicted in Fig. 2.

The proposed methodology has been developed under the following assumptions.

- 1) Only additive or bias faults are considered for both the actuator and the active suspension sensors, attempting to represent abrupt and incipient faults, $\dot{f} = 0$ [49].
- 2) Due to the extremely low probability of two simultaneous faults occurring, it is assumed that only a single component may be faulty at any given time during the operation, whether it is the actuator or a sensor.

A. UIO Design for Sensors Faults Estimation: UIO-SF

As mentioned in Section II-C, both sensor and actuator faults cannot be estimated using a single observer for this system, as the number of measurements is lower than the number of potential faults (10). For that reason, in order to have an estimation of actuator and sensor faults, two different UIO are proposed, using one for the estimation of sensor faults (UIO-SF) and the other one for

the estimation of actuator faults (UIO-AF), satisfying in this way the conditions in (10). From (5), and expanding the state vector to consider f_s and its derivative $\bar{x}_s(t) = [x^T(t) \quad \dot{f}_s^T(t) \quad f_s^T(t)]^T$, it leads to

$$\begin{aligned} \dot{\bar{x}}_s(t) &= \bar{A}_d \bar{x}_s(t) + \bar{B}_d u(t) + \bar{B}_{d,\omega} \omega(t) \\ y(t) &= \bar{C} \bar{x}_s(t) + D u(t) + D_\omega \omega(t) \end{aligned} \quad (11)$$

where

$$\begin{aligned} \bar{A} &= \begin{bmatrix} A & 0 & 0 \\ 0 & 0 & 0 \\ 0 & I & 0 \end{bmatrix}, \quad \bar{B} = \begin{bmatrix} B \\ 0 \\ 0 \end{bmatrix}, \quad \bar{B}_{d,\omega} = \begin{bmatrix} B_\omega \\ 0 \\ 0 \end{bmatrix} \\ \bar{C} &= [C \quad 0 \quad I]. \end{aligned} \quad (12)$$

For the design of the UIO-SF, the system in (11) is discretized as follows:

$$\begin{aligned} \bar{x}_s(k+1) &= A_d \bar{x}_s(k) + B_d u(k) + B_{d,\omega} \omega(k) \\ y(k) &= C x(k) + D u(k) + D_\omega \omega(k) \end{aligned} \quad (13)$$

where

$$\bar{A}_d = I + T_s \bar{A}, \quad \bar{B}_d = T_s \bar{B}, \quad \bar{B}_{d,\omega} = T_s \bar{B}_\omega$$

and T_s is the sample time. The UIO dynamics for the estimation of $\bar{x}_s(k)$ is

$$\begin{aligned} \bar{z}_s(k+1) &= R_s \bar{z}_s(k) + X_s u(k) + K_s (y(k) - D u(k)) \\ \hat{\bar{x}}_s(k) &= \bar{z}_s(k) + H_s (y(k) - D u(k)) \end{aligned} \quad (14)$$

where \bar{z}_s is the state vector of the observer and R_s , X_s , K_s , and H_s are the matrices of the observer to be found and $\hat{\bar{x}}_s(k)$ is the estimation of $\bar{x}_s(k)$.

By defining the estimation error as

$$e(k) = \bar{x}_s - \hat{x}_s \quad (15)$$

and using (14), $e(k)$ can be expressed as

$$\begin{aligned} e(k) &= \bar{x}_s(k) - \hat{x}_s(k) \\ &= (I - H_s \bar{C}) \bar{x}_s(k) - z_s(k) - H_s D_\omega \omega_k. \end{aligned} \quad (16)$$

By taking the derivative of the error we get

$$\begin{aligned} e(k+1) &= (I - H_s \bar{C}) \bar{x}_s(k+1) \\ &\quad - \bar{z}_s(k+1) - H_s D_\omega \omega(k+1). \end{aligned} \quad (17)$$

Using (11) into (17) we obtain

$$\begin{aligned} e(k+1) &= (I - H_s \bar{C})(\bar{A} \bar{x}_s(k) + \bar{B} u(k) + \bar{B}_\omega \omega(k)) \\ &\quad - (R_s \bar{z}_s + X_s \bar{B} u(k) + K_s (y(k) - D u(k))) \\ &\quad - H_s D_\omega \omega(k+1). \end{aligned} \quad (18)$$

By defining $K_s = K_{s,1} + K_{s,2}$ and $N_s = I - H_s \bar{C}$ and using (16), the estimation error $e(k+1)$ can be expressed as

$$\begin{aligned} e(k+1) &= N_s \bar{A} \bar{x}_s(k) + ((N_s \bar{B} - X_s) u(k) \\ &\quad + N_s (\bar{B}_\omega - K_{s,1} D_d) \omega(k)) \\ &\quad - R_s \bar{z}_s(k) - K_{s,1} \bar{C} \bar{x}_s(k) \\ &\quad - K_{s,2} (y(k) - D u(k)) \\ &\quad - H_s D_\omega \omega(k+1). \end{aligned} \quad (19)$$

By imposing the following conditions:

$$\begin{aligned} R_s &= N_s \bar{A}_d - K_{s,1} \bar{C} \\ X_s &= N_s B_d \\ K_{s,2} &= R_s H_s \\ K_s &= K_{s,1} + K_{s,2} \end{aligned} \quad (20)$$

one can get (19) reduced to

$$\begin{aligned} e(k+1) &= (I - H_s \bar{C}) \bar{A} - K_{s,1} \bar{C} \bar{e}(k) \\ &\quad + (N_s \bar{B}_\omega - K_{s,1} D_d) \omega(k) - H_s D_\omega \omega(k+1). \end{aligned} \quad (21)$$

It can be seen that if conditions in (20) are satisfied, the error dynamics is only influenced by the external input perturbances $\omega(k)$ and $\omega(k+1)$. To deal with these perturbances, a new perturbation vector is defined as

$$d(k) = \begin{bmatrix} \omega(k) \\ \omega(k+1) \end{bmatrix} \quad (22)$$

and the expression (21) can be rewritten as

$$e(k+1) = (N_s \bar{A} - K_{s,1} \bar{C}) \bar{e}(k) + W d(k) \quad (23)$$

where

$$W = [N_s \bar{B}_\omega - K_{s,1} D_d \quad -H_s D_\omega]. \quad (24)$$

The design of the observer must reduce the influence of the disturbances caused by road irregularities into the estimation

error by an attenuation index γ to minimize

$$\|e\|_2^2 < \gamma^2 \|d\|_2^2. \quad (25)$$

Theorem 2: Given the matrices R_s , X_s , K_s , and H_s of the appropriate dimensions, there exists an UIO of the form shown in (14), which is asymptotically stable and guarantees the \mathcal{H}_∞ performance described in (25) if there is a matrix $P = P^\top \succ 0$, Q and Y such that

Proof: By choosing a Lyapunov function of the form

$$V(k) = e^\top(k) P e(k) \quad (27)$$

where $P = P^\top \succ 0$ to satisfy $V(k) > 0$ and $V(k+1) - V(k) < 0$ must be hold for the system to be asymptotically stable. To achieve stability and guarantee the \mathcal{H}_∞ condition in (25) with a performance index γ , the following inequality must be hold:

$$\begin{aligned} e^\top(k+1) P e(k+1) - e^\top(k) P e(k) + e^\top(k) e(k) \\ - d^\top(k) \gamma^2 d(k) < 0. \end{aligned} \quad (28)$$

Using (21), the inequality (28) can be rewritten in LMI form as

$$\begin{bmatrix} \Upsilon - P + I & \star \\ W^\top P (N_s \bar{A} - K_{s,1} \bar{C}) & -\gamma^2 I + W^\top P W \end{bmatrix} \prec 0 \quad (29)$$

where $\Upsilon = (N_s \bar{A} - K_{s,1} \bar{C})^\top P (N_s \bar{A} - K_{s,1} \bar{C})$. Applying Schur's complement and using (20) and (24) and defining $Q = P K_{s,1}$ and $Y = P H_s$ we get (26) shown at the bottom of next page, and the proof is concluded. ■

The gains of the objective controller are found by solving the minimization problem

$$\begin{aligned} \min \gamma^2 \\ \text{subject to } P = P^\top \succ 0, \end{aligned} \quad (30)$$

Finally, using (20) the matrices of the observer can be found.

B. UIO Design for Actuator Fault Estimation: UIO-AF

The procedure for estimating actuator fault is the same as the UIO-SF. In this case, the expanded state vector contains the actuator fault f_a and its derivative $\bar{x}_a(t) = [x^\top(t) \quad \dot{f}_a^\top(t) \quad f_a^\top(t)]^\top$ the system is

$$\begin{aligned} \dot{\bar{x}}_a(t) &= \tilde{A} \bar{x}_a(t) + \bar{B} u(t) + \bar{B}_\omega \omega(t) \\ y(t) &= \tilde{C} \bar{x}_a(t) + D u(t) + D_\omega \omega(t) \end{aligned} \quad (31)$$

where

$$\begin{aligned} \tilde{A}_d &= \begin{bmatrix} A_d & 0 & B_d \\ 0 & 0 & 0 \\ 0 & I & 0 \end{bmatrix} \\ \tilde{C}_a &= [C \quad 0 \quad D]. \end{aligned}$$

After applying the Euler method as in (13), the observer dynamics for the estimation of the states of (31) are

$$\begin{aligned} \bar{z}_a(k+1) &= R_a \bar{z}_a(k) + X_a u(k) + K_a (y(k) - D u(k)) \\ \hat{\bar{x}}_a(k) &= \bar{z}_a(k) + H_a (y(k) - D u(k)) \end{aligned} \quad (32)$$

TABLE I
 DETECTION OF UIOS TO FAULTS

Current Fault	UIO-SF FD	UIO-AF FD
f_a	$\hat{f}_{\Delta_z, \text{UIO}}$	$\hat{f}_{a, \text{UIO}}$
f_{Δ_z}	$\hat{f}_{\Delta_z, \text{UIO}}$	$\hat{f}_{a, \text{UIO}}$
$f_{\dot{z}_s}$	$\hat{f}_{\dot{z}_s, \text{UIO}}$	—
$f_{\dot{z}_u}$	$\hat{f}_{\dot{z}_u, \text{UIO}}$	$\hat{f}_{a, \text{UIO}}$

where \bar{z}_a is the state vector of the observer and R_a , X_a , K_a , and H_a are the matrices of the UIO to be found. Using the same procedure as in Section III-A and Theorem 2, the matrices of the observer in (32) can be found so that the stability of the observer is guaranteed with a performance index γ_a .

C. Deflection Sensor and Actuator Fault Coupling

Although two UIOs are designed in order to estimate separately the sensor and the actuator faults, there exists a problem of coupling between the observers. As the UIO-SF only considers that the system is solely subject to sensor faults, it will be considered a sensor fault when an actuator fault occurs. The same happens for the UIO-AF, it considers sensors faults as actuator faults. This phenomenon is summarized in Table I, where the sensibility of the observers to the faults is shown.

It can be appreciated that both $f_{\dot{z}_s, \text{UIO}}$ and $f_{\dot{z}_u, \text{UIO}}$ can be isolated by only considering the estimations made by the UIO-SF. However, the same does not apply to $f_{a, \text{UIO}}$ and $f_{\Delta_z, \text{UIO}}$ as they are coupled: the UIO-SF considers f_a as a deflection sensor fault and the UIO-AF considers $f_{\Delta_z, \text{UIO}}$ as an actuator fault. To solve this issue, a switch OFF detector is proposed: when the estimation given by the UIO-SF $\hat{f}_{\Delta_z, \text{UIO}}$, which is sensitive to both $f_{a, \text{UIO}}$ and $f_{\Delta_z, \text{UIO}}$, exceeds a predefined threshold, the actuator is switched OFF by setting a trigger signal to 1 as depicted in Fig. 2. In order to determine the origin of the fault, the actuator is disconnected so that the possible fault caused by it do not longer affect the system. In this way, if the fault estimation persists above the threshold value once the actuator is switched OFF, it means that the fault comes from the sensor and the flag signal $\text{flag}_{\Delta_z, \text{pre}}$ is triggered. Otherwise, the fault is coming from the actuator. In this case, $\text{flag}_{f_a, \text{pre}}$ is triggered. The activation of the switch OFF mechanism depends on the estimation $\hat{f}_{\Delta_z, \text{UIO}}$, which is provided by UIO which is robust to road the system disturbances. This estimation must be held above a predefined threshold for a specific time to activate the switching OFF mechanism, thus preventing false positive caused by road disturbances. By switching OFF the actuator, the suspension becomes a passive suspension, which is stable and thus there is no danger that the system will become unstable. The complete process is described in detail in Fig. 3. In order to treat

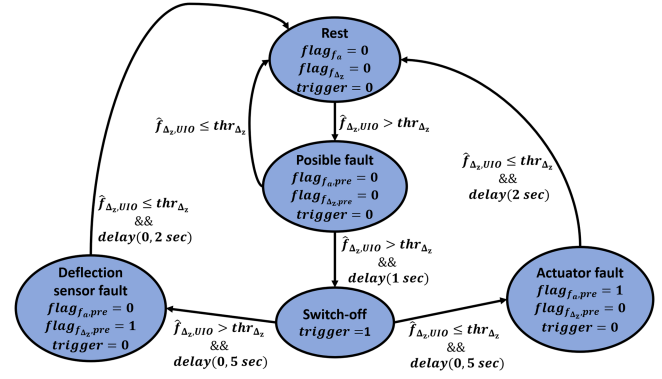


Fig. 3. Switch OFF mechanism scheme.

noisy signals, the $f_{\Delta_z, \text{UIO}}$ signal is used after being smoothed out using a sliding window technique.

D. Flag Generation for FD

Once the fault is identified, the flags for the faults detection are generated using the outputs of the UIOs ($\hat{f}_{a, \text{UIO}}$, $\hat{f}_{\Delta_z, \text{UIO}}$, $\hat{f}_{\dot{z}_s, \text{UIO}}$, $\hat{f}_{\dot{z}_u, \text{UIO}}$) and the flags given by the switch OFF mechanism $\text{flag}_{\Delta_z, \text{pre}}$, $\text{flag}_{f_a, \text{pre}}$, as detailed in Algorithm 1.

To avoid false positives in the flags that indicate whether a fault occurs, an exponential moving average algorithm (EMA) [50] is applied to these signals, so that the results are more robust against false positives and avoids rapid and repeated changes in the detections, (33). Since the value of EMA is not boolean, the corresponding flag will be set to 1 if the EMA value exceeds a predefined upper threshold, to 0 if it falls under a predefined lower threshold and remains unchanged in the dead zone between the thresholds, see Fig. 4.

$$\text{EMA}_{j,t} = \alpha_j \text{flag}_{j,t} + \text{EMA}_{j,t-1} (1 - \alpha)$$

$$\text{for } j = f_a, f_{\Delta_z}, f_{\dot{z}_s}, f_{\dot{z}_u} \quad (33)$$

$$\text{flag}_{j,t} = \begin{cases} 1 & \text{for } \text{EMA}_{j,t} > \epsilon_{\text{upper},j} \\ 0 & \text{for } \text{EMA}_{j,t} < \epsilon_{\text{lower},j} \\ \text{flag}_{j,t-1} & \text{otherwise} \end{cases}$$

$$\text{for } j = f_a, f_{\Delta_z}, f_{\dot{z}_s}, f_{\dot{z}_u} \quad (34)$$

where $\epsilon_{\text{upper},j}$ and $\epsilon_{\text{lower},j}$ are the upper and lower threshold for the EMA, respectively.

E. Fault Estimation Correction

From the observers described above, an *a priori* estimation of the faults is obtained, $\hat{f}_{\text{UIO}} = [\hat{f}_{a, \text{UIO}} \ \hat{f}_{\Delta_z, \text{UIO}} \ \hat{f}_{\dot{z}_s, \text{UIO}} \ \hat{f}_{\dot{z}_u, \text{UIO}}]^T$. As the estimation faults will be coupled, it

$$\begin{bmatrix} -P + I & * & * & * \\ 0 & -\gamma^2 I & * & * \\ 0 & 0 & -\gamma^2 I & * \\ P\bar{A} - Y\bar{C} \bar{A} - Q\bar{C} & P\bar{B}_\omega - Y\bar{C} \bar{B}_\omega - QD_d^T & -YD_\omega & -P \end{bmatrix} \prec 0. \quad (26)$$

Algorithm 1: Generation of Flags for Fault Detection.

Require: $\hat{f}_{a,UIO}, \hat{f}_{\Delta_z,UIO}, \hat{f}_{\ddot{z}_s,UIO}, \hat{f}_{\ddot{z}_u,UIO},$
 $flag_{\Delta_z,pre}, flag_{f_a,pre};$
Ensure: $flag_{f_a}, flag_{f_{\Delta_z}}, flag_{f_{\ddot{z}_s}}, flag_{f_{\ddot{z}_u}};$
 $flag_{f_a} \leftarrow 0;$
 $flag_{f_{\Delta_z}} \leftarrow 0;$
 $flag_{f_{\ddot{z}_s}} \leftarrow 0;$
 $flag_{f_{\ddot{z}_u}} \leftarrow 0;$
while $k \neq N_{total\ samples}$ **do**
 if $\hat{f}_{\ddot{z}_s,UIO}(k) \geq \epsilon_{\ddot{z}_s}$ **then**
 $flag_{f_{\ddot{z}_s}}(k) \leftarrow 1$
 else
 $flag_{f_{\ddot{z}_s}}(k) \leftarrow 0$
 end if
 if $\hat{f}_{\ddot{z}_u,UIO}(k) \geq \epsilon_{\ddot{z}_u}$ **then**
 $flag_{f_{\ddot{z}_u}}(k) \leftarrow 1$
 else
 $flag_{f_{\ddot{z}_u}}(k) \leftarrow 0$
 end if
 if $\hat{f}_{\Delta_z,UIO}(k) \geq \epsilon_{\Delta_z} \ \& \ flag_{\Delta_z,pre}$ **then**
 $flag_{f_{\Delta_z}}(k) \leftarrow 1$
 else
 $flag_{f_{\Delta_z}}(k) \leftarrow 0$
 end if
 if $\hat{f}_{f_a,UIO}(k) \geq \epsilon_{f_a} \ \& \ flag_{f_a,pre}(k)$ **then**
 $flag_{f_a}(k) \leftarrow 1$
 else
 $flag_{f_a}(k) \leftarrow 0$
 end if
 $k \leftarrow k + 1;$
end while

is necessary to only consider the estimation result using the detection of the corresponding fault as depicted in Fig. 2. Thus, the final estimation of the faults $\hat{f} = [\hat{f}_a \ \hat{f}_{\Delta_z} \ \hat{f}_{\ddot{z}_s} \ \hat{f}_{\ddot{z}_u}]^T$ is calculated as

$$\hat{f} = \mathcal{K} \hat{f}_{UIO} \quad (35)$$

where \mathcal{K} is the masking system matrix defined as follows:

$$\mathcal{K} = \begin{bmatrix} flag_{f_a} & 0 & 0 & 0 \\ 0 & flag_{\Delta_z} & 0 & 0 \\ 0 & 0 & flag_{\ddot{z}_s} & 0 \\ 0 & 0 & 0 & flag_{\ddot{z}_u} \end{bmatrix}. \quad (36)$$

F. MPC-Based Active Suspension Control

The ASS is controlled using a model predictive controller, which control law is defined as follows:

$$u(k + N|k) = F(k)x(k + N|k) \quad (37)$$

where N is the finite horizon of the MPC, $u(k + N|k)$ is the control input force for the next N time instants of the actuator to the system, and $F(k)$ is the control gain to be found by solving

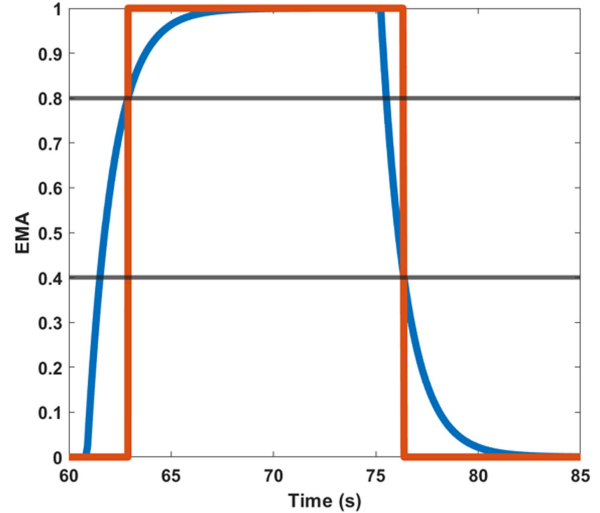


Fig. 4. EMA performance.

the cost function minimization problem

$$J(k) = \sum_{i=0}^N (\dot{z}_s^\top(k+i|k)Q\dot{z}_s(k+i|k) + u^\top(k+i|k)Ru(k+i|k)) \quad (38)$$

where Q and R are the weighting matrices to design. The objective is to minimize the cost function in (38) subject to the maximum allowable applied force of the actuator and the maximum deflection that the suspension can withstand due to its physical limitations. The optimization problem to solve is described in (39).

In this work, the offline MPC approach is used as in [16] to calculate the feedback gain $F(k)$ offline and reduce the online calculations significantly

$$\begin{cases} \min_{F(k)} J(k) \\ \text{subject to:} \\ |u(k)| < u_{\max}, |x_s - x_u| < \Delta z_{\max} \end{cases} \quad (39)$$

As the states of the model cannot be measured directly, the estimations of the states given by the UIO-SF are used. The state estimates provided by the UIO-SF are chosen to feed the controller over UIO-AF because it takes into account measurement faults to correct the state estimations, while the UIO-AF is sensitive to these, resulting in poor state estimates.

IV. RESULTS AND DISCUSSION

In this section, the proposed fault diagnosis methodology is tested to prove its effectiveness via simulation using *MATLAB* and *CarSim* software, a vehicle dynamics simulation software extensively used by automotive companies and universities research labs. Initially, the simulation is conducted using *MATLAB*, where the vehicle plant is equivalent to the model used for the design of the UIOs, a 2-DoF vehicle model. Afterward, simulations on a 27-DoF vehicle model plant in *CarSim* are carried out in order to prove the effectiveness of the methodology

TABLE II
DEFINITION OF PARAMETERS OF THE ASS

Symbol	Description	Value	Unit
m_s	Quarter sprung mass	451.12	kg
m_u	Quarter unsprung mass	40	kg
k_s	Spring stiffness	43000	N/m
c_s	Damper coefficient	1500	Ns/m
k_u	Tire spring stiffness	230000	N/m
c_u	Tire damping coefficient	14.60	Ns/m
u_{\max}	Max. actuator force	2500	N
Δz_{\max}	Max. suspension deflection	40	mm

TABLE III
THRESHOLD VALUES

Threshold	Description	Value
ϵ_{f_a}	Threshold for f_a	150.0 N
$\epsilon_{f_{\Delta z}}$	Threshold for $f_{\Delta z}$	8.0 mm
$\epsilon_{f_{\ddot{z}_s}}$	Threshold for $f_{\ddot{z}_s}$	1.0 m/s ²
$\epsilon_{f_{\ddot{z}_u}}$	Threshold for $f_{\ddot{z}_u}$	2.1 m/s ²

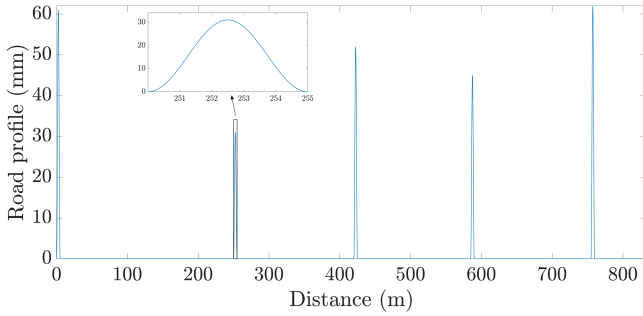


Fig. 5. Road profile scenario I.

on a full suspension vehicle model, which is different from the quarter suspension model used for the design of the UIOs.

A. Case A: Quarter Suspension Vehicle Model

The characteristics of the linear quarter car model in (1) are described in Table II.

The model simulation is carried out at a frequency of 100 Hz. Abrupt faults in sensors and actuators are considered, see Fig. 8.

To estimate the fault values, UIO-SF and UIO-AF matrices are found by solving conditions in (30) for the system of (5). The optimization problem is solved using Robust Control Toolbox included in *MATLAB*. Feasible solutions were found for a performance index of $\gamma = 5$ and $\gamma_a = 11$ for UIO-SF and UIO-AF, respectively.

The fixed thresholds are defined empirically as in [41] for the detection of the actuator and sensor faults are shown in Table III.

The fault diagnosis scheme for the ASS is tested in two typical scenarios used to test the performance of a vehicle suspension: a road with bumps and a high-speed road. The road profile for the first scenario, see Fig. 5, whose bumps profiles are defined as [23]

$$z_r(t) = \begin{cases} \frac{A}{2} [1 - \cos(\frac{2\pi L}{V}(t - t_{\text{start}}))] \\ \text{for } t_{\text{start}} + L/V \geq t \geq t_{\text{start}} \\ 0 \text{ otherwise} \end{cases} \quad (40)$$

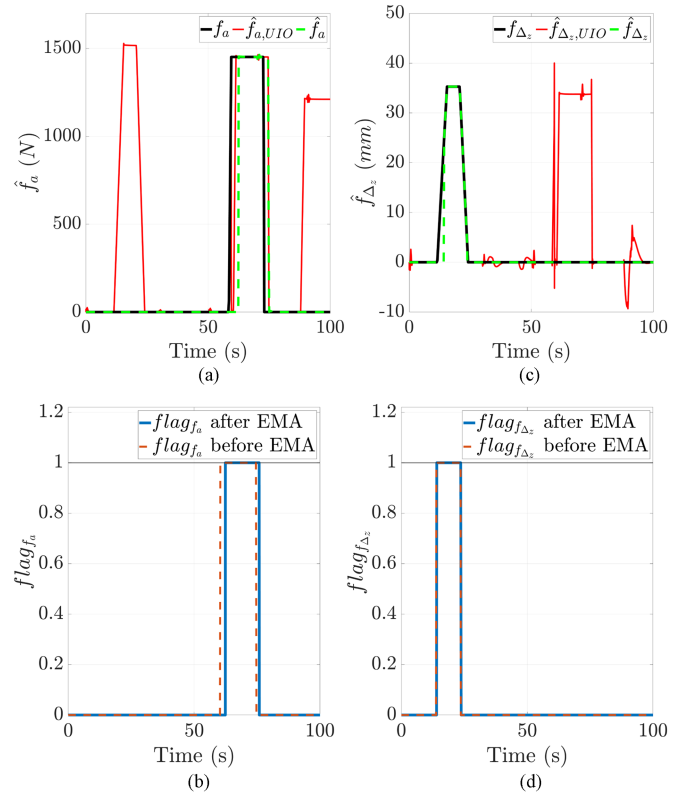


Fig. 6. Case A, Scenario I. (a) Actuator fault (black) pre-masked estimation (red) and post-masked estimation (green). (b) Actuator FD. (c) Deflection sensor fault (black) pre-masked estimation (red) and post-masked estimation (green). (d) Deflection sensor FD.

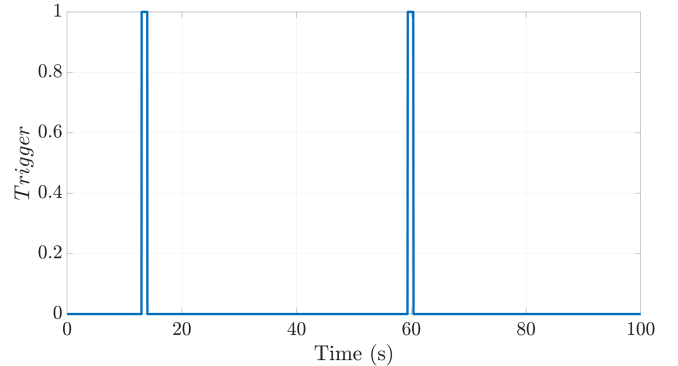


Fig. 7. Actuator trigger signal for Case A, Scenario I.

where the bump length is $L = 5$ m, the vehicle longitudinal velocity is $V = 45$ km/h for this scenario and t_{start} is the starting time of the bump. A road like this has been chosen for the vehicle to travel over bumps while faults occur. In Fig. 8, the profiles of the faults produced in the actuator and sensors are depicted.

The trigger signals to switch OFF the actuator are shown in Fig. 7, where it can be appreciated that they are set to 1 when the deflection sensor and actuator faults are produced. In Fig. 6(a)–(c), the estimations pre-masked (red) and post-masked (green) of the actuator and deflection sensor faults are shown. One can see in Fig. 6(a) that the UIO-AF is sensitive to deflection sensor

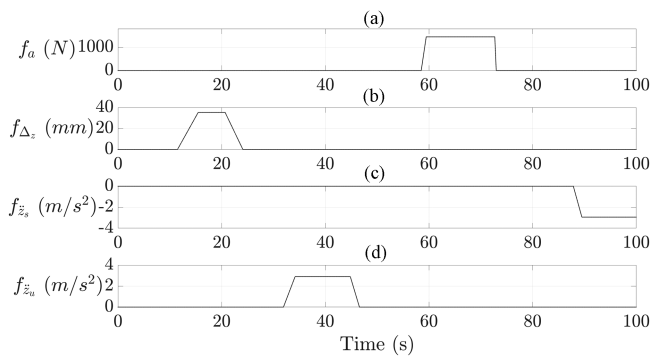


Fig. 8. Faults produced in the system. (a) Actuator. (b) Deflection sensor. (c) Sprung mass accelerometer. (d) Unsprung mass accelerometer.

fault at 12 s and to sprung mass acceleration sensor at 87 s of the simulation, emphasizing the coupling issue between fault estimations and the importance of the use of the masking system to filter these false estimations.

Also, in Fig. 6(c), it can be appreciated that the premasked estimation given by the UIO-SF of $\hat{f}_{\Delta_z,UIO}$ (red) is sensitive to the actuator fault, pointing out once again the problem of fault coupling detection and nonstrong detectability conditions explained in Sections II-C and III-C. In Fig. 6(b)–(d), it can be seen that the detections flags of these faults given by the switch OFFmechanism allows to distinguish the origin of the fault, as corrected estimation \hat{f}_{f_a} and \hat{f}_{Δ_z} (green) fits with the real fault values (black). Furthermore, there are no false positive detections.

The estimations of the sprung mass and unsprung mass accelerations sensors faults are depicted in Fig. 9(a) and (c), respectively. In these cases, the premasked estimations $\hat{f}_{\ddot{z}_s,UIO}$ and $\hat{f}_{\ddot{z}_u,UIO}$ (red) are not sensitive to the actuator fault. The detection of both sensors faults matches the instants at which the faults occur, Fig. 9(b) and (d). It can be appreciated the robustness of the UIOs in Figs. 6(a), 6(c), 9(a), and 9(c), as the road disturbances do not affect significantly to the premasked estimations (red). Anyway, the logic masking system corrects these wrong estimations caused by the road bumps and the EMA algorithm filter a false detection at 60 s.

The Scenario II road profile consists of a random profile that has been generated following the ISO 8608 [51] standard for a road Class-A, see Fig. 10. The vehicle speed for this case is $V = 100\text{km/h}$. The fault profiles are the same as first scenario, see Fig. 8. As the fault occurs at the same times as in the previous scenario, the trigger has disabled the actuator at the same instants, see Fig. 11.

The estimations of the actuator fault can be seen in Fig. 12(a). The premasked estimation $\hat{f}_{a,UIO}$ (red) is sensitive again to the deflection sensor fault and sprung mass accelerometer fault. The postmasked estimation \hat{f}_a (green) shows a very close estimate of the value of the actuator fault (black). The detection of the actuator fault shows robustness against the road disturbances as there are no false positives at any time, see Fig. 12(b). The estimations of the deflection sensor faults are displayed in Fig. 12(c), where it can be seen that the premasked estimation $\hat{f}_{\Delta_z,UIO}$

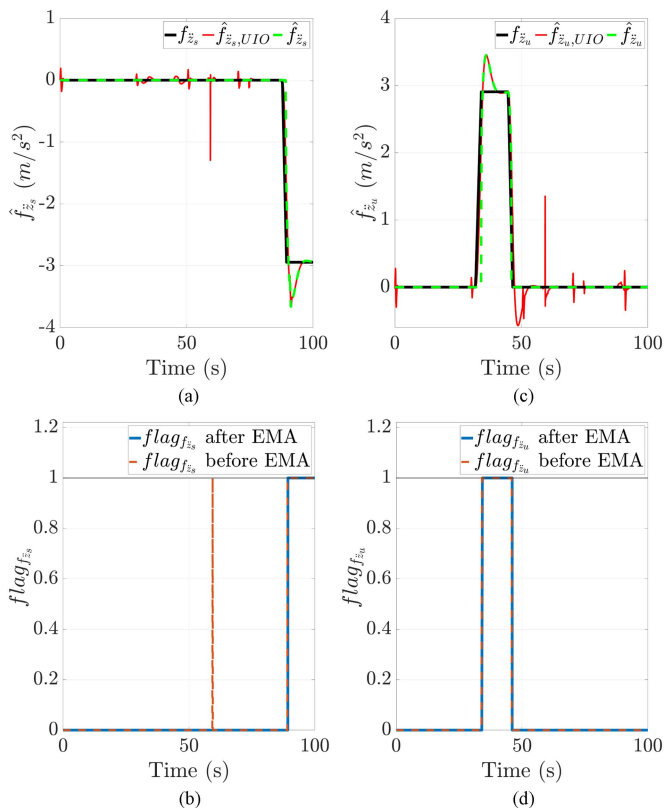


Fig. 9. Case A, Scenario I. (a) Sprung mass accelerometer sensor fault (black) premasked estimation (red) and postmasked estimation (green). (b) Sprung mass accelerometer sensor FD. (c) Unsprung mass accelerometer sensor fault (black) premasked estimation (red) and postmasked estimation (green). (d) Unsprung mass accelerometer sensor FD.

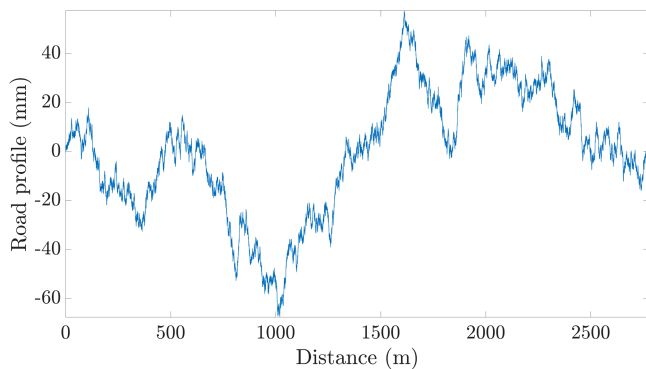


Fig. 10. Road profile for Scenario II.

(red) indicates once more the sensitivity of the estimation to the actuator fault. As in the previous scenario, the flag generated by the switch OFFmechanism allows to identify the fault and correct the estimations given by the UIOs.

Fig. 13 displays the estimations and the detections of sprung mass and unsprung mass accelerometers faults, respectively. In this case, it can be seen in Fig. 13(a) and (c) that the premasked estimations (red) do not present false positives and they are robust to road disturbances. The postmasked estimations (green) only present a nonzero value when positive detection,

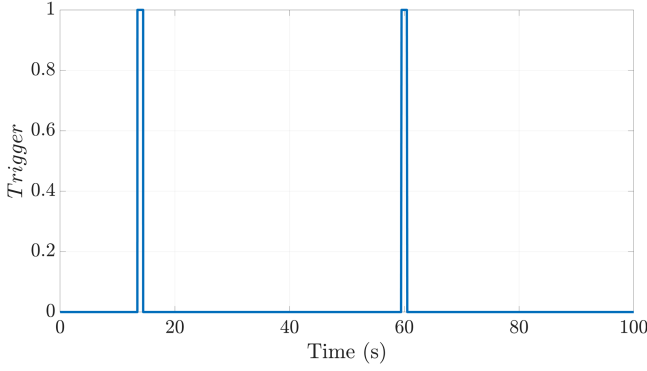


Fig. 11. Actuator trigger signal for Case A, Scenario II.

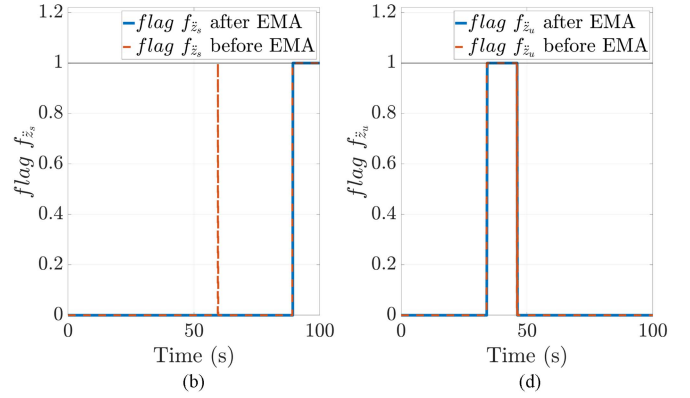
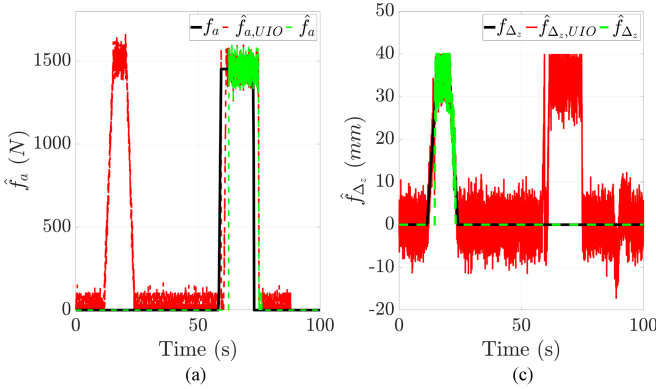
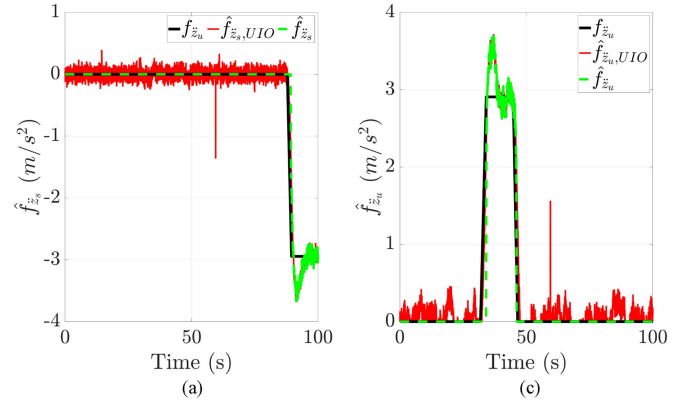


Fig. 13. Case A, Scenario II. (a) Sprung mass accelerometer sensor fault (black) premasked estimation (red) and postmasked estimation (green). (b) Sprung mass accelerometer sensor FD. (c) Unsprung mass accelerometer sensor fault (black) premasked estimation (red) and postmasked estimation (green). (d) Unsprung mass accelerometer sensor FD.

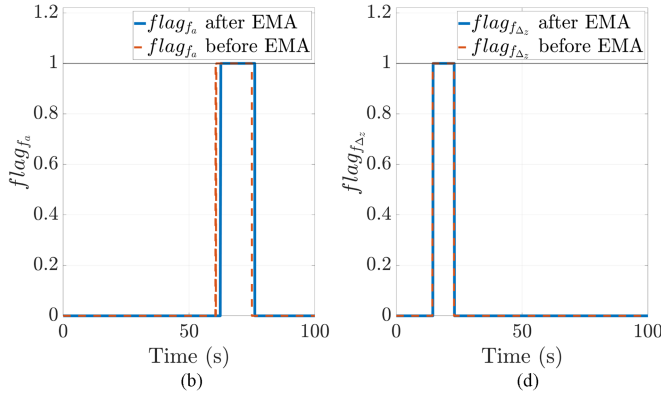


Fig. 12. Case A, Scenario II. (a) Actuator fault (black) premasked estimation (red) and postmasked estimation (green). (b) Actuator FD. (c) Deflection sensor fault (black) premasked estimation (red) and postmasked estimation (green). (d) deflection sensor FD.

see Fig. 13(b) and (d). At 60 s, it can be appreciated how the EMA algorithm filters a false positive detection of the sprung mass acceleration sensor, see Fig. 13(c).

B. Case B: Full Suspension Vehicle Model

The previous results show that the proposed methodology works for a linear quarter-model, where an ideal environment is reproduced. To validate its performance in a more realistic scenario, the same tests are conducted using the vehicle dynamics simulation software, which allows to run simulations using a 27-DOF vehicle model.

Fig. 14(a) shows the estimation and detection of the actuator fault, where it can be seen that the fault is fully detected in both scenarios. However, the estimation of the fault provided by the UIO-AF does not correspond to the real value of the fault. Apart from the nonlinearities of the *CarSim* vehicle model, the estimation error is caused by the difference between the model used for the design of the UIOs and the *CarSim* plant model. The quarter suspension vehicle model considers a significantly smaller sprung mass than the full vehicle model. In addition, the *CarSim* model is a full suspension model where there are four independent suspension systems. This coupling between the suspensions through the sprung mass avoids an accurate estimation of the actuator fault, as the extra force provided by the actuator due to its fault is absorbed by the suspensions of other wheels.

In this case, the trigger signal is not shown as is very similar to the one shown in Figs. 7 and 11. The results obtained for the deflection sensor for the road with bumps and scenario II using *CarSim* are shown in Fig. 14(c), where the detections of the faults match the moment of the fault and the coupling with the actuator fault is not considered, as in the quarter suspension model results. It is remarkable that in this case, the UIOs are more sensitive to the bumps as in the quarter car model. This is again due to the difference between the model used to design the UIOs and the plant model.

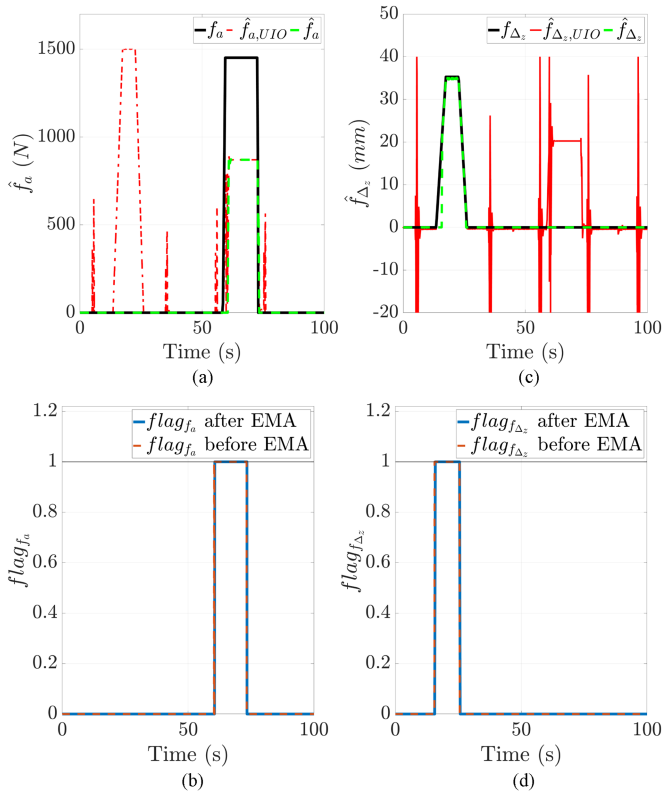


Fig. 14. Case B, Scenario I. (a) Actuator fault (black) premasked estimation (red) and postmasked estimation (green). (b) Actuator FD. (c) Deflection sensor fault (black) premasked estimation (red) and postmasked estimation (green). (d) Deflection sensor FD.

TABLE IV
ESTIMATION ERROR

RMSE/SMAPE	Quarter vehicle model				CarSim model			
	Scenario 1		Scenario 2		Scenario 1		Scenario 2	
	RMSE	SMAPE	RMSE	SMAPE	RMSE	SMAPE	RMSE	SMAPE
$f_a - \hat{f}_a$ (N)	10.42	10.09%	50.29	10.61%	580.31	11.24%	495.61	15.31%
$f_{\Delta_z} - \hat{f}_{\Delta_z}$ (mm)	0.04	5.84%	3.38	8.87%	0.40	5.67%	4.67	7.40%
$\dot{f}_{z_u} - \hat{\dot{f}}_{z_u}$ (m/s^2)	0.345	3.69%	0.34	3.78%	0.65	3.27%	0.19	2.19%
$\dot{f}_{z_s} - \hat{\dot{f}}_{z_s}$ (m/s^2)	0.34	6.68%	0.42	6.73%	0.30	6.62%	0.19	2.33%

Finally, Figs. 15 and 17 show the estimation and detection of the sprung mass and unsprung mass acceleration sensors, respectively. One can see similar results compared with the obtained using the quarter suspension vehicle model. However, there are short detections when the car passes the bumps, but it can be appreciated the work done by the EMA by eliminating these possible false detections in Fig. 17(b) and (c).

In Fig. 16, it can be appreciated that the UIOs estimations are too noisy due to the road disturbance. Despite the noise, the estimations follow the value of the fault and the detection flags are generated correctly. Finally, in Fig. 17, the estimations and detections of the faults in the sprung and unsprung mass accelerometers are shown, where similar results as in the road with bumps scenario are obtained.

In Table IV, a summary of the root mean square error (RMSE) and the symmetric mean absolute percentage error (SMAPE) of the estimation calculated as in (41) is shown. It can be appreciated that the RMSE for the actuator fault and deflection sensor fault are larger for the *CarSim*. These differences are

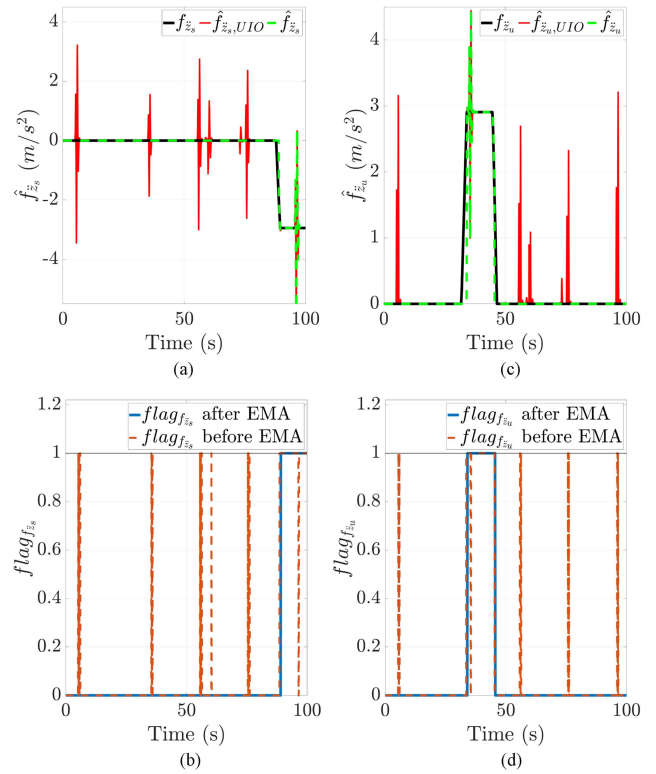


Fig. 15. Case B, Scenario I. (a) Sprung mass accelerometer sensor fault (black) premasked estimation (red) and postmasked estimation (green). (b) Sprung mass accelerometer sensor FD. (c) Unsprung mass accelerometer sensor fault (black) premasked estimation (red) and postmasked estimation (green). (d) Unsprung mass accelerometer sensor FD.

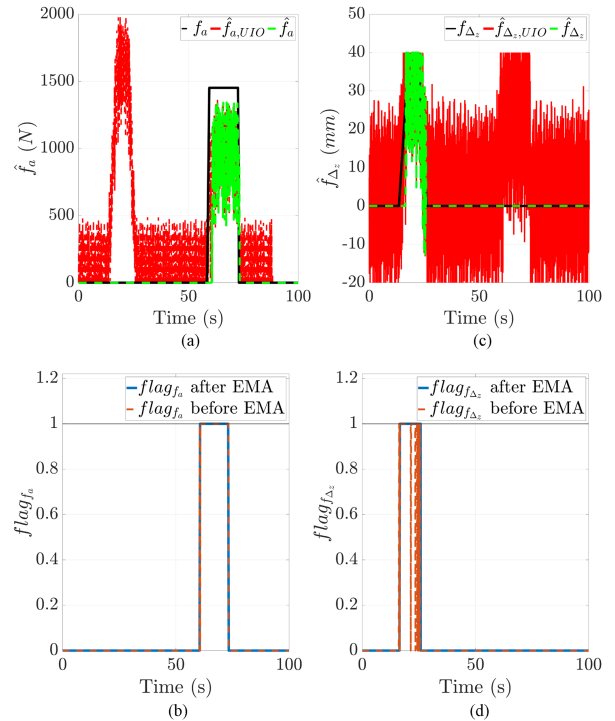


Fig. 16. Case B, Scenario II. (a) Actuator fault (black) premasked estimation (red) and postmasked estimation (green). (b) Actuator FD. (c) Deflection sensor fault (black) premasked estimation (red) and postmasked estimation (green). (d) Deflection sensor FD.

TABLE V
COMPARISON WITH OTHER WORKS

Methodology	Actuator faults f_a		Sensor faults f_s	
	Result	Type	Result	Type
Proposed in [28], [31]	✓	Additive + gain	✗	–
Proposed in [34], [42]	✓✓	Additive + gain	✗	–
Proposed in [30], [41]	✗	–	✓	Additive
Proposed in [33], [40]	✗	–	✓✓	Additive
Proposed methodology (quarter suspension vehicle model)	✓✓	Additive	✓✓	Additive
Proposed methodology (full suspension vehicle model)	✓✓	Additive	✓✓	Additive

✗ Not considered, ✓ Detection, ✓✓ Detection and estimation.

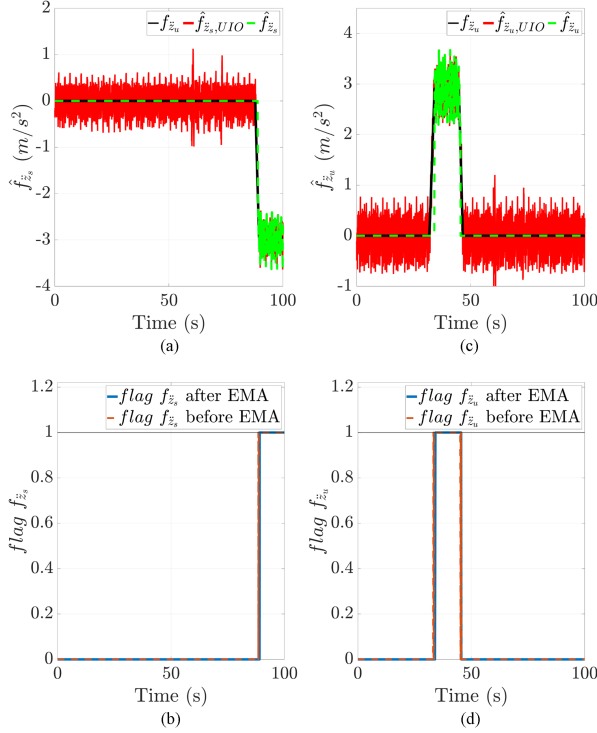


Fig. 17. Case B, Scenario II. (a) Sprung mass accelerometer sensor fault (black) premasked estimation (red) and postmasked estimation (green). (b) Sprung mass accelerometer sensor FD. (c) Unsprung mass accelerometer sensor fault (black) premasked estimation (red) and postmasked estimation (green). (d) Unsprung mass accelerometer sensor FD.

mainly caused by the difference between the model used for the design of the observers and the full vehicle *CarSim* model. *CarSim* simulations are used to prove that the observers can work properly with a high-order model even though the UIOs has been designed from a low-order suspension model. The first one considers a linear model with only one wheel affected only by the road disturbances of it, while in the *CarSim* model the other suspensions have effects on the one where the fault is detected through the movement of the chassis due to pitch and roll dynamics, causing more severe disturbances and reducing the estimation performance of the observers. Scenario I cases offer better estimation on the deflection sensor fault for both cases, as the system excitation of the road disturbances in this Scenario is much lower. On the other hand, the estimations of the sprung and unsprung masses acceleration are lower for *CarSim* simulations. This is mainly caused by the difference on the mass

		Actual fault					
		No fault	f_a	f_{Δ_z}	f_{z_s}	f_{z_u}	
Detected fault	No fault	4570 83.30%	208 3.79%	275 5.01%	121 2.21%	312 5.69%	83.30%
	f_a	40 3.13%	1239 96.87%	0 0.00%	0 0.00%	0 0.00%	96.87%
	f_{Δ_z}	0 0.00%	0 0.00%	987 100.00%	0 0.00%	0 0.00%	100.00%
	f_{z_s}	0 0.00%	0 0.00%	0 0.00%	1094 100.00%	0 0.00%	100.00%
	f_{z_u}	0 0.00%	0 0.00%	0 0.00%	0 0.00%	1154 100.00%	100.00%
		99.13%	85.63%	78.21%	90.04%	78.72%	90.44%

Fig. 18. Case B, Scenario I. Confusion matrix.

		Actual fault					
		No fault	f_a	f_{Δ_z}	f_{z_s}	f_{z_u}	
Detected fault	No fault	4456 83.70%	388 7.29%	291 5.47%	87 1.63%	102 1.92%	83.70%
	f_a	154 12.70%	1059 87.30%	0 0.00%	0 0.00%	0 0.00%	87.30%
	f_{Δ_z}	0 0.00%	0 0.00%	971 100.00%	0 0.00%	0 0.00%	100.00%
	f_{z_s}	0 0.00%	0 0.00%	0 0.00%	1128 100.00%	0 0.00%	100.00%
	f_{z_u}	0 0.00%	0 0.00%	0 0.00%	0 0.00%	1364 100.00%	100.00%
		96.66%	73.19%	76.94%	92.84%	93.04%	89.78%

Fig. 19. Case B, Scenario II. Confusion matrix.

of the vehicle and the mass considered on the design of the UIOs, which allows to damp the estimation and avoid the overshooting behavior shown in Figs. 9 and 13. The SMAPE never exceeds the 16% for actuator and the 9% for any sensor

$$\begin{aligned}
 \text{RMSE} &= \sqrt{\sum_{k=1}^N \frac{(f_{i,k} - \hat{f}_{i,k})^2}{N}} \\
 \text{SMAPE} &= \frac{\sum_{k=1}^N 2 \frac{|f_{i,k} - \hat{f}_{i,k}|}{|f_{i,k}| + |\hat{f}_{i,k}|}}{N} \\
 &\text{for } f_i = f_a, f_{\Delta_z}, f_{z_s}, f_{z_u}. \quad (41)
 \end{aligned}$$

Figs. 18 and 19 show, respectively, the confusion matrix for the detections of the faults. As can be seen, in both scenarios the overall accuracy is near to 90%, and only “no fault” and “actuator fault” categories are under 100% accuracy. All the misidentified cases are due to delay time that takes for the proposed methodology to identify the origin of the faults emphasized by EMA algorithm, which can be appreciated to have a greater impact on the detections of faults in the actuator.

As can be seen from the results, both actuator and sensor faults are detected using the novel proposed fault diagnosis scheme in contrast with previous works, as shown in Table V.

V. CONCLUSION

This article proposed a novel approach to overcome the FD problem in ASSs. As faults can occur in the actuator and any sensor, strong detectability conditions can never be satisfied, so no single observer or residual generator can be used for both fault estimation and detection. For that reason, a novel fault diagnosis methodology to simultaneously estimate the actuator and sensor faults is presented in this work. First, two separate robust UIOs are designed using \mathcal{H}_∞ theory in order to independently estimate the sensors and actuator faults. As there exists coupling between some faults, they cannot be isolated using the UIOs information. By using a novel switching OFF mechanism, the actuator is deactivated so the fault can be identified. Finally, flags are generated to indicate which component is faulty and they are used to correct the previous estimations of the UIOs. The proposed methodology is tested in two typical road scenarios (bumps and high-speed) for two vehicle system plants with different complexity (2-DoF and 27-DoF vehicle models). Numerical results show that the proposed methodology is able to detect and estimate actuator and sensor faults for both scenarios, in contrast with previous works. Future research will focus on determining thresholds based on vehicle characteristics to adapt the mechanism to different suspension models, as well as detecting and estimating additional types of faults, such as stuck or gain faults.

REFERENCES

- [1] F. Zhu, Y. Tang, and Z. Wang, "Interval-observer-based fault detection and isolation design for t-s fuzzy system based on zonotope analysis," *IEEE Trans. Fuzzy Syst.*, vol. 30, no. 4, pp. 945–955, Apr. 2022.
- [2] F. Viadero-Monasterio, B. L. Boada, H. Zhang, and M. J. L. Boada, "Integral-based event triggering actuator fault-tolerant control for an active suspension system under a networked communication scheme," *IEEE Trans. Veh. Technol.*, vol. 72, no. 11, pp. 13848–13860, Nov. 2023.
- [3] H. E. Tseng and D. Hrovat, "State of the art survey: Active and semi-active suspension control," *Veh. Syst. Dyn.*, vol. 53, no. 7, pp. 1034–1062, 2015.
- [4] A. Alfidhli, J. Darling, and A. J. Hillis, "The control of an active seat with vehicle suspension preview information," *J. Vib. Control*, vol. 24, no. 8, pp. 1412–1426, 2018.
- [5] J. Kumar and G. Bhushan, "Dynamic analysis of quarter car model with semi-active suspension based on combination of magneto-rheological materials," *Int. J. Dyn. Control*, vol. 11, no. 2, pp. 482–490, 2023. [Online]. Available: <https://link.springer.com/10.1007/s40435-022-01024-1>
- [6] F. Viadero-Monasterio, A. T. Nguyen, J. Lauber, M. J. L. Boada, and B. L. Boada, "Event-triggered robust path tracking control considering roll stability under network-induced delays for autonomous vehicles," *IEEE Trans. Intell. Transp. Syst.*, vol. 24, no. 12, pp. 14743–14756, Dec. 2023.
- [7] J. Na, Y. Huang, Q. Pei, X. Wu, G. Gao, and G. Li, "Active suspension control of full-car systems without function approximation," *IEEE/ASME Trans. Mechatron.*, vol. 25, no. 2, pp. 779–791, Apr. 2020.
- [8] D. Ning, H. Du, N. Zhang, S. Sun, and W. Li, "Controllable electrically interconnected suspension system for improving vehicle vibration performance," *IEEE/ASME Trans. Mechatron.*, vol. 25, no. 2, pp. 859–871, Apr. 2020.
- [9] M. Jurisch, "Vertical trajectory planning: An optimal control approach for active suspension systems in autonomous vehicles," *Veh. System Dyn.*, vol. 60, no. 11, pp. 3788–3809, 2022.
- [10] L.-H. Zong, X.-L. Gong, S.-H. Xuan, and C.-Y. Guo, "Semi-active H_∞ control of high-speed railway vehicle suspension with magnetorheological dampers," *Veh. System Dyn.*, vol. 51, no. 5, pp. 600–626, 2013.
- [11] G. Wang, C. Chen, and S. Yu, "Optimization and static output-feedback control for half-car active suspensions with constrained information," *J. Sound Vib.*, vol. 378, pp. 1–13, 2016.
- [12] H. Pan, X. Jing, and W. Sun, "Robust finite-time tracking control for nonlinear suspension systems via disturbance compensation," *Mech. Syst. Signal Process.*, vol. 88, pp. 49–61, 2017.
- [13] J. N. Strohm and F. Christ, "Preview H_∞ control of a hybrid suspension system," *IFAC-PapersOnLine*, vol. 52, no. 5, pp. 237–242, 2019.
- [14] P. Brezas and M. C. Smith, "Linear quadratic optimal and risk-sensitive control for vehicle active suspensions," *IEEE Trans. Control Syst. Technol.*, vol. 22, no. 2, pp. 543–556, Mar., 2014.
- [15] L. V. V. G. Rao and S. Narayanan, "Optimal response of half car vehicle model with sky-hook damper based on LQR control," *Int. J. Dyn. Control*, vol. 8, no. 2, pp. 488–496, 6 2020.
- [16] S. M. Moradi, A. Akbari, and M. Mirzaei, "An offline LMI-based robust model predictive control of vehicle active suspension system with parameter uncertainty," *Trans. Inst. Meas. Control*, vol. 41, no. 6, pp. 1699–1711, 2019.
- [17] D. Rodriguez-Guevara, A. Favela-Contreras, F. Beltran-Carbajal, D. Sotelo, and C. Sotelo, "Active suspension control using an MPC-LQR-LPV controller with attraction sets and quadratic stability conditions," *Mathematics*, vol. 9, no. 20, pp. 1–17, 2021.
- [18] D. Hernández-Alcántara, J. C. Tudón-Martínez, L. Amézquita-Brooks, C. A. Vivas-López, and R. Morales-Menéndez, "Modeling, diagnosis and estimation of actuator faults in vehicle suspensions," *Control Eng. Pract.*, vol. 49, pp. 173–186, 2016.
- [19] M. Moradi and A. Fekih, "A stability guaranteed robust fault tolerant control design for vehicle suspension systems subject to actuator faults and disturbances," *IEEE Trans. Control Syst. Technol.*, vol. 23, no. 3, pp. 1164–1171, May 2015.
- [20] R. Wang, H. Jing, H. R. Karimi, and N. Chen, "Robust fault-tolerant H_∞ control of active suspension systems with finite-frequency constraint," *Mech. Syst. Signal Process.*, vol. 62/63, pp. 341–355, 2015.
- [21] J. Xiong, X. Chang, J. H. Park, and Z. Li, "Nonfragile fault-tolerant control of suspension systems subject to input quantization and actuator fault," *Int. J. Robust Nonlinear Control*, vol. 30, no. 16, pp. 6720–6743, 2020.
- [22] H. Pan, C. Zhang, and W. Sun, "Fault-tolerant multiplayer tracking control for autonomous vehicle via model-free adaptive dynamic programming," *IEEE Trans. Rel.*, vol. 72, no. 4, pp. 1395–1406, Dec. 2022.
- [23] F. Viadero-Monasterio, B. Boada, M. Boada, and V. Díaz, " H_∞ dynamic output feedback control for a networked control active suspension system under actuator faults," *Mech. Syst. Signal Process.*, vol. 162, 2022, Art. no. 108050.
- [24] H. Kim and H. Lee, "Fault-tolerant control algorithm for a four-corner closed-loop air suspension system," *IEEE Trans. Ind. Electron.*, vol. 58, no. 10, pp. 4866–4879, Oct. 2011.
- [25] J. Jiang, *Robust Model-Based Fault Diagnosis for Dynamic Systems*. Boston, MA, USA: Springer, 2002.
- [26] S. X. Ding, *Model-Based Fault Diagnosis Techniques*, 2nd ed. London, U.K: Springer, 2013.
- [27] W. Na, C. Park, S. Lee, S. Yu, and H. Lee, "Sensitivity-based fault detection and isolation algorithm for road vehicle chassis sensors," *Sensors*, vol. 18, no. 8, 2018, Art. no. 2720.
- [28] S. Yan, W. Sun, F. He, and J. Yao, "Adaptive fault detection and isolation for active suspension systems with model uncertainties," *IEEE Trans. Rel.*, vol. 68, no. 3, pp. 927–937, Sep. 2019.
- [29] X. Zhu, Y. Xia, S. Chai, and P. Shi, "Fault detection for vehicle active suspension systems in finite-frequency domain," *IET Control Theory Appl.*, vol. 13, no. 3, pp. 387–394, 2019.
- [30] Z. Mao, Y. Zhan, G. Tao, B. Jiang, and X. G. Yan, "Sensor fault detection for rail vehicle suspension systems with disturbances and stochastic noises," *IEEE Trans. Veh. Technol.*, vol. 66, no. 6, pp. 4691–4705, Jun. 2017.
- [31] S. M. H. Rizvi, M. Abid, and A. Q. Khan, "Actuator fault diagnosis and isolation in vehicle active suspension system," in *Proc. IEEE 9th Int. Conf. Emerg. Technol.*, 2013, pp. 1–6.
- [32] Y. P. S. Kumaran, C. P. Tan, Y. S. Chiew, and W.-S. Chua, "Remaining useful life estimation for high speed industrial robots using an unknown input observer for feature extraction," *IEEE Trans. Rel.*, vol. 72, no. 3, pp. 1018–1028, Sep. 2023.

- [33] A. Abboudi, S. Bououden, M. Chadli, I. Boukhaibet, and B. Neji, "Observer-based fault-tolerant predictive control for LPV systems with sensor faults: An active car suspension application," *Appl. Sci.*, vol. 12, no. 2, 2022, Art. no. 684.
- [34] M. M. Morato, O. Sename, L. Dugard, and M. Q. Nguyen, "Fault estimation for automotive electro-rheological dampers: LPV-based observer approach," *Control Eng. Pract.*, vol. 85, pp. 11–22, 2019.
- [35] X. Du, G. Han, M. Yu, Y. Peng, X. Xu, and J. Fu, "Fault detection and fault tolerant control of vehicle semi-active suspension system with magneto-rheological damper," *Smart Mater. Structures*, vol. 30, no. 1, 2021, Art. no. 014004.
- [36] D. Hernandez-Alcantara, R. Morales-Menendez, and L. Amezcua-Brooks, "Fault detection for automotive shock absorber," in *J. Physics: Conf. Ser.*, vol. 659, no. 1, p. 012037, 2015.
- [37] A. Chamseddine, H. Noura, and M. Ouladsine, "Sensor fault detection, identification and fault tolerant control: Application to active suspension," in *Proc. Amer. Control Conf.*, 2006, Art. no. 6.
- [38] X. Jiang, X. Xu, and H. Shan, "Model-based fault diagnosis of actuators in electronically controlled air suspension system," *World Electric Veh. J.*, vol. 13, no. 11, 2022, Art. no. 219.
- [39] C. Sadhukhan, S. K. Mitra, M. K. Naskar, and M. Sharifpur, "Fault diagnosis of a nonlinear hybrid system using adaptive unscented kalman filter bank," *Eng. Comput.*, vol. 38, no. 3, pp. 2717–2728, 2022. [Online]. Available: <https://link.springer.com/10.1007/s00366-020-01235-0>
- [40] Z. Ye, H. Ni, Z. Xu, and D. Zhang, "Sensor fault estimation of networked vehicle suspension system with deny-of-service attack," *IET Intell. Transport Syst.*, vol. 14, no. 5, pp. 455–462, 2020.
- [41] K. Jeong, S. B. Choi, and H. Choi, "Sensor fault detection and isolation using a support vector machine for vehicle suspension systems," *IEEE Trans. Veh. Technol.*, vol. 69, no. 4, pp. 3852–3863, Apr. 2020.
- [42] P. Jin, W. Xue, and K. Li, "Actuator fault estimation for vehicle active suspensions based on adaptive observer and genetic algorithm," *Shock Vib.*, vol. 2019, 2019, Art. no. 1783850.
- [43] H. Dimassi, "A novel fault reconstruction and estimation approach for a class of systems subject to actuator and sensor faults under relaxed assumptions," *ISA Trans.*, vol. 111, pp. 192–210, 2021.
- [44] M. Pazera, M. Witczak, N. Kukurowski, and M. Buciakowski, "Towards simultaneous actuator and sensor faults estimation for a class of takagi-sugeno fuzzy systems: A twin-rotor system application," *Sensors*, vol. 20, no. 12, pp. 1–18, 2020.
- [45] K. Bansal, P. Dahiya, and P. Mukhija, "Event-triggered based reliable control of vehicle active suspension system under actuator faults," *IFAC-PapersOnLine*, vol. 51, no. 1, pp. 196–201, 2018.
- [46] J. Kasprzyk, P. Krauze, S. Budzan, and J. Rzepecki, "Vibration control in semi-active suspension of the experimental off-road vehicle using information about suspension deflection," *Arch. Control Sci.*, vol. 27, pp. 251–261, 2017.
- [47] M. Hautus, "Strong detectability and observers," *Linear Algebra Appl.*, vol. 50, pp. 353–368, 1983.
- [48] M. Darouach, M. Zasadzinski, and S. Xu, "Full-order observers for linear systems with unknown inputs," *IEEE Trans. Autom. Control*, vol. 39, no. 3, pp. 606–609, Mar. 1994.
- [49] Z. Gao, X. Liu, and M. Z. Chen, "Unknown input observer-based robust fault estimation for systems corrupted by partially decoupled disturbances," *IEEE Trans. Ind. Electron.*, vol. 63, no. 4, pp. 2537–2547, Apr. 2016.
- [50] F. Klinker, "Exponential moving average versus moving exponential average," *Mathematische Semesterberichte*, vol. 58, pp. 97–107, 2011.
- [51] ISO 8608:2016(E), *Mechanical Vibration — Road Surface Profiles — Reporting of Measured Data*, Geneva, CH, Switzerland: International Organization for Standardization, Nov. 2016.



Miguel Meléndez-Useros (Student Member, IEEE) received the B.S. degree in industrial engineering and the M.S. degree in industrial engineering from Universidad Carlos III de Madrid (UC3M), Madrid, Spain, in 2020 and 2022, respectively. He is currently working toward the Ph.D. degree in fault detection and estimation and fault tolerant control for vehicles with the Department of Mechanical Engineering, UC3M.

He joined the Department of Mechanical Engineering, UC3M, in 2020. His research areas include vehicle dynamics, vehicle safety, control systems and fault-tolerant control, and fault detection.



Manuel Jiménez-Salas (Student Member, IEEE) received the B.S. degree in industrial engineering from Universidad de Malaga (UMA), Malaga, Spain, in 2019, the M.S. degree in industrial engineering from Universidad Carlos III de Madrid (UC3M), Madrid, Spain, in 2021. He is working toward the Ph.D. degree in vehicle trajectory tracking with Department of Mechanical Engineering, UC3M.

He joined the Department of Mechanical Engineering, UC3M, in 2019. His research areas include vehicle dynamics, vehicle safety, control systems, and

path following control.



Fernando Viadero-Monasterio (Member, IEEE) received the B.S. degree in industrial engineering from Universidad de Cantabria (UNICAN), Santander, Spain, in 2018, the M.S. degree in industrial engineering and the Ph.D. degree in mechanical engineering from University Carlos III de Madrid (UC3M), Madrid, Spain, in 2020 and 2023, respectively.

He joined the Department of Mechanical Engineering, UC3M, in 2018. His research areas include vehicle dynamics, vehicle safety, control systems, fault-tolerant control and non-linear systems.

Dr. Viadero-Monasterio is a member of IFToMM Technical Committee for Transportation Machinery.



María Jesús López-Boada received the industrial engineering degree and the Ph.D. degree in industrial technologies from University Carlos III de Madrid (UC3M), Madrid, Spain, in 1996 and 2002, respectively.

From 1997 to 2002, she was a Research and Teaching Assistant with the Department of Systems and Automation Engineering, UC3M. In 2002, she joined the Department of Mechanical Engineering, UC3M. Since 2020, she is currently a Full Professor and is co-responsible of the Research Group Advanced

Vehicle Dynamics and Mechatronic Systems (VEDYMEC). Her research interests include artificial neural networks, control systems, Kalman filters, system dynamics modeling, sensor fusion, vehicle safety, advanced vehicle dynamics, MR dampers, and bus structures.